Inductively Coupled Plasmas as Atomization Cells for Atomic Fluorescence Spectrometry

Akbar Montaser and Velmer A. Fassel*

Ames Laboratory—ERDA and Department of Chemistry, Iowa State University, Ames, Iowa 50010

Inductively coupled plasmas (ICP) offer promise as atomization cells for atomic fluorescence spectrometry (AFS). In this study, an ICP formed part of a modular spectroscopic system for atomic fluorescence, emission, and absorption measurements. Details on the assembly of the complete system are provided. Microwave-excited, thermostated, electrodeless discharge lamps were used as primary sources for exciting the atomic fluorescence. A minicomputer provided control of radiofrequency (RF) forward power and site of observation in the plasma, as well as data acquisition and processing. The effects of important variables on the plasma background, the atomic fluorescence signal, and signal-to-noise ratio were examined. Scattering and matrix effects were also evaluated. The atomic fluorescence powers of detection for Cd, Zn, and Hg were found to be superior to those observed in emission when the same experimental facilities were used for the measurements.

Inductively coupled plasmas (ICP) have been shown to be promising atomization and excitation sources for atomic emission spectrometry (AES) (For recent reviews, see references *1*, *2*, and *3*.) When the free atoms or ions in an ICP are observed in emission, the detection limits for many elements are in the range of 0.0001 to 15 ng/ml. Sequential or true simultaneous multielement determinations may be performed with minimal interelement effects. In spite of the excellent powers of detection achievable, there are a number of elements (Hg, Sn, Te, As, Bi, Se, Te) which play an important role in biomedicine, nutrition, and environmental pollution at concentration levels below those now determinable by ICP-AES techniques. All of these elements possess resonance lines with wavelengths less than 300 nm. For these wavelengths, observation of the free atoms in fluorescence should, in principle, lead to superior powers of detection if sufficiently intense primary excitation sources are available (*4*–*7*). Most previous investigations on the analytical utility of atomic fluorescence (AF) have been performed with hydrogen–air or hydrogen–oxygen–argon combustion flame atomization cells. In these flames, incomplete sample volatilization has resulted in severe solute vaporization interferences and scattering of the primary source radiation. These flames have therefore been restricted to situations in which relatively volatile elements are contained in essentially matrix-free solutions (*7*). The higher temperature nitrous oxide–acetylene flame has also been utilized, but the high background emission from this flame and fluorescence quenching by the combustion products have necessitated the use of lasers as primary excitation sources (*6*, *7*).

There are several reasons why an ICP may prove to be a more useful atomization cell for atomic fluorescence spectrometry (AFS) than combustion flames. First, the combination of high temperature and relatively long analyte–plasma interaction times in the plasma leads to a high degree of volatilization and atomization and a consequent increase in freedom from physical and chemical interferences. Second, the high volatilization and atomization efficiencies achieved in an ICP should minimize scattering of the primary radiation, regardless of the type of primary excitation source utilized. Third, the argon coolant and aerosol-carrier gas employed in the ICP provides a chemically-inert environment that possesses a small quenching cross section as well.

In this paper, the ICP is introduced as an atomization cell for AFS. In the sections that follow, the design and construction of a modular, computer-controlled ICP atomic fluorescence, emission, and absorption spectroscopic system is described. AF detection limits for elements such as Cd, Zn, and Hg, for which relatively intense primary excitation sources (PES) are available, are presented and compared to the best results so far obtained for atomic emission (AE) ICP systems. An evaluation of the scattering and matrix effect interferences in the AFS-ICP system is also presented.

INSTRUMENTATION

The AFS-AES-AAS spectrometer was operated under the control of a minicomputer that was interfaced to an eight-channel, multiplexer/analog-to-digital converter (ADC), two programmable stepper motor controllers, and the RF power supply. For all of the interfacing, a Heath minicomputer interface system was employed with appropriate circuit cards. The software was written in assembly language (MACRO-8). The components of the system are described in Table I and below.

Optical System. All of the optical components were positioned on a stable, T-shape table so that atomic fluorescence, emission, and absorption investigations could be conducted with a single facility. The plasma atomization cell, described below, was positioned between the two monochromators, one of which was suitable for atomic emission observations while the other provided a higher aperture more appropriate for AFS. The focal lengths of the two monochromators were 1.0 m and 0.25 m, respectively. The primary excitation sources for AFS were mounted at right angles to the optical axis of the two monochromators. For atomic absorption observations, the 0.25-meter monochromator may be replaced by the proper PES.

The optical table, designed and constructed in this laboratory, consisted of three table tops, made of sandstone, and the table base. The two monochromators and the optical rails were all mounted on leveling pads (P306B, Vlier Leveling Pad, Iowa Industrial Products, Des Moines, Iowa) and were firmly held on the table tops by means of 15-cm long "U" clamps (No. 499A716, McMaster-Carr Supply Co., Chicago, Ill.) and proper bolts which penetrated through the table tops.

Two external optical systems were designed to match the effective apertures of the spectrometers and the diameter of the photomultiplier photocathode surface. For the AFS optimization studies, a 1-cm long by 0.3-cm wide image of the PES was formed at the plasma central axis by means of a two-lens system. A mechanical light chopper was positioned between the two lenses, one of which formed an intermediate image on the chopper. The entrance slits of both spectrometers were located 42 cm from the vertical axis of the plasma torch. A 1:1 image of the plasma itself was formed on the entrance slit of each monochromator with a lens. An adjustable

Table I. Experimental Facilities

Components	Description and supplier
Minicomputer System	Model PDP-8/E-AE computer (Digital Equipment Corp., Maynard, Mass.) with 8K core, a DK8-EP Programmable Real-Time Clock and a KA8-E External Interface for Positive I/O Devices. The system contains a model ASR-33 teletype.
Multiplexer/Analog-to-Digital Converter	Model 721-122-100-08-S-3, 12-bit (Zeltex, Inc. Concord, Calif.).
Minicomputer Interface System	Model EU-801E with all appropriate circuit cards (Heath Co., Benton Harbor, Mich.).
Scanning Monochromator/Spectrograph	Model 78-466 (Jarrell-Ash Co., Waltham, Mass.), with 1180 grooves/mm grating blazed for 250 nm; adjustable straight entrance and exit slits.
Quarter-Meter Monochromator	Model 82-410 (Jarrell-Ash Co., Waltham, Mass.), with 300-nm blaze, 2360 grooves/mm grating. Both entrance and exit slits were straight bayonet type and are fixed, 1 mm wide and 20 mm long.
Photomultiplier Tube	Type 6256B (EMI Gencom Inc., Plainview, N.Y.), 13-stage tube with S-13 response.
Lens System	Spherical plano-convex lenses made of fused quartz or Suprasil having diameter of 3–5 cm. Only Suprasil lenses were utilized for the primary excitation source optical system.
Mechanical Light Chopper	Model 125 (Princeton Applied Research Corp., Princeton, N.J.)
Osram Lamp PES System	Hg, Zn, and Cd lamps with power supply (George W. Gate & Co., Inc., Long Island, N.Y.); air cooling of lamps improved the AF radiance.
Perkin-Elmer PES System	The system consists of 30-W power supply and a Cd lamp. The recommended power level for Cd is 5 W. The system is not thermostated (Perkin-Elmer Co., Norwalk, Conn.).
Stepping Motors and Controllers	Model SM-2A (Denco Research Inc., Tucson, Ariz.). The system was operated in the switch activated initialization mode for both on and off line operations.
Ratio Frequency Generator and Impedance Matching Network	Model 3000 PGB/27 MHz (Henry Electronics, Los Angeles, Calif.). The generator provides forward powers of up to 3 kW at oscillation frequency 27.125 MHz. The impedance matching network was modified as described in the text.
Preamplifier and Remote Adaptor	Type A (Princeton Applied Research Corp., Princeton, N.J.).
Lock-in Amplifier	Model HR-8 (Princeton Applied Research Corp., Princeton, N.J.).

diaphragm placed on each lens allowed matching of the lens and monochromator apertures. The entrance lenses were enclosed in blackened tubes extending from the vicinity of the plasma to the spectrometer entrance slits to reduce the level of extraneous room and plasma radiation entering the spectrometer. For AE observations, the light chopper was placed between the spectrometer and the entrance lens. The blackened tube was not used in this case.

To determine the AFS detection limits and the linear dynamic concentration ranges, a single-lens system was utilized to form an ~3 cm^2 (3-cm long, 1-cm wide) image of the PES in the plasma. The mechanical chopper was mounted between the PES and the lens. An entrance lens with a magnification of 1/3 was used to transfer the optical fluorescence from the plasma to either of the two spectrometers.

Primary Excitation Sources (PES). Because of our particular interest in evaluating the ICP-AFS approach for elements whose sensitive lines occur at wavelengths less than 250 nm, we did not consider pulsed tunable dye lasers (*8–12*), even with frequency doubling or mixing, as viable PES's. Therefore, the next most intense sources—microwave excited electrodeless discharge lamps (EDL's) and Osram lamps—were employed. The EDL's were excited with an A-antenna in a thermostated housing (*13*). The thermostated EDL device consisted of a heater, an EDL lamp unit, a microwave power supply, and the associated coupling device and electronics.

Heater Unit. Two 24-ohm (600 W) nichrome wire coils were placed in the slots of a ceramic plate (A-4 plate made of ceramic with 10 slots, Blue M Electric Co., Blue Island, Ill.) located inside a box made of maranite. The electrical leads of the two coils were connected to two different zones (each rated at 600 W) of a proportional temperature controller (Model 2155-40, Cole-Parmer Instrument Co., Chicago, Ill.). The temperature sensor (Model 2157-60, Cole-Parmer Instrument Co.) was a platinum wire encased in a stainless steel sheath. The temperature sensor was normally positioned near the heater element to prevent coupling to the A-antenna. With no high frequency power applied to the A-antenna, the same temperatures were measured when the sensor was attached either to the lamp, or positioned near the heater elements. A small electric fan circulated the air inside the maranite box. The furnace reached a maximum equilibrium temperature of 800 °C in about 30 min. Because of the high temperature of the furnace, the bottom section of the A-antenna was water cooled, which also reduced the reflected power.

EDL Lamp Unit. All lamps were obtained from either the Ophthos Instrument Co. (Rockville, Md.) or from other investigators (as identified in Table III). The lamp was inserted in a double O-ring clamp and was mounted firmly in the furnace so that the tip of the lamp was located about 1 mm above the antenna stub. Direct contact between the antenna stub and the EDL was avoided to prevent discoloration of the quartz tube. Lamp changes could be accomplished in a few seconds. The lamp radiation emerged through a quartz window in the furnace housing.

Microwave Power Supply, Coupling, Device, and Associated Electronics. Microwave power to the thermostated device was provided by a 125-W, 2450-MHz unit (Microtherm Model CMD5, Raytheon Manufacturing Co., Waltham, Mass.). An A-antenna (Model 2254-5002G1, Sorensen Co., Manchester, N.H.) was utilized for microwave coupling with the lamp. The generator output was sent to a separate reflected-power meter (Model 725.3, Microwave Devices, Inc., Farmington, Conn.), then to a 0.9-meter coaxial cable (Type 57-111G2E, Raytheon Service Co., Newton Upper Falls, Mass.), which was connected to the A-antenna.

Atomization System. *Plasma Torch Assembly.* The X, Y, and Z stages of this assembly provided three-dimensional

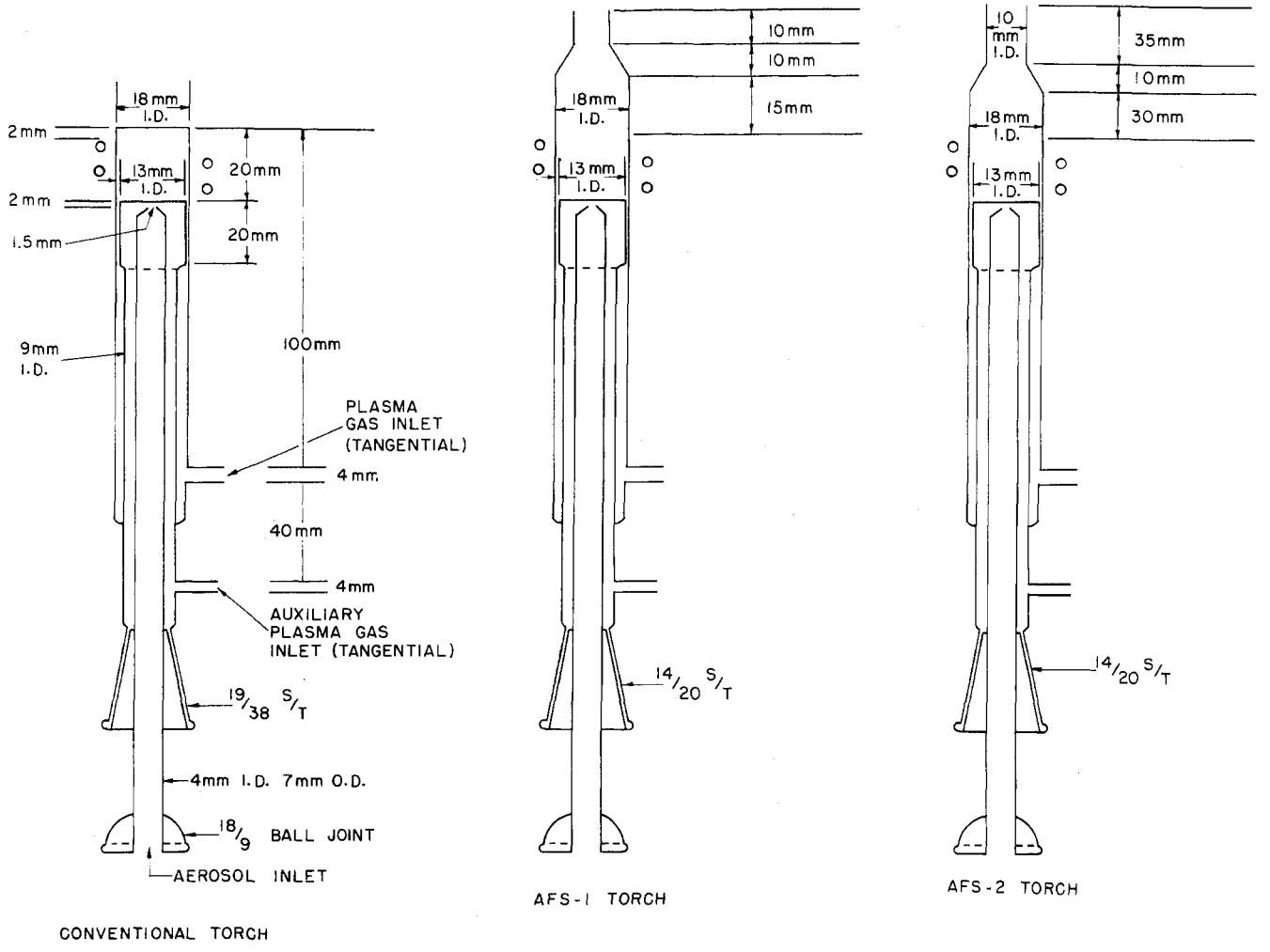

Figure 1. Plasma torch dimensions

positioning of the entire plasma torch system, i.e., the plasma torch, the nebulizer and spray chamber, and the impedance matching network for the RF generator. To reduce RF interference with other instrumentation, a blackened galvanized sheet-metal housing surrounded the plasma torch. Three adjustable windows in the housing allowed the two monochromators to view the plasma as well as providing a path for PES radiation to excite the atomic vapor. The impedance matching network was mounted on auxiliary X′–Y′ stages, which in turn were attached to the Z stage of the plasma torch assembly. Because the load coil was attached to the impedance matching network, fine adjustment of the X′–Y′ stage changed the position of the load coil with respect to the torch axial center. This configuration was helpful in the formation of a symmetrical plasma. The motion of the Y and Z stages was directed by two stepping motors. Two programmable stepper-motor controllers provided highly accurate (2% nonaccumulative error) reproducible rotary motion for positioning these stages. The Y stage scanned the plasma torch in front of the spectrometer entrance slit and could travel a distance of 3.5 cm. The Z stage provided a vertical motion of about 10 cm. The resolution of these two stages was about 6.35 μm/step. The position of the X stage, which scanned the plasma torch in front of the PES over a distance of 2.5 cm for atomic fluorescence observations was controlled by a handcrank.

The programmable controllers provided initialization to ensure knowledge of the exact position of each motor. In the INTERNAL mode of operation, the operator entered the address(es) of the desired position(s) of the Y stage and/or Z stage via a switch register. The controller internal memory kept track of each motor location following each subsequent motion. In the EXTERNAL mode, an internal memory latch allowed the computer to load an address location and then dropped "off-line" while the controller moved the motor. When the motor arrived at the desired location, a flag output signaled the computer.

Plasma Torch Designs. Plasma AE measurements have usually been performed in this laboratory at an observation height of 15 to 25 mm above the load coil. As will be demonstrated in a later section, measurements of AF in this height range were not feasible because of strong plasma background and analyte emission. With the usual torch designs (*14*), the tail flame disperses and expands at distances greater than 25 mm above the load coil to cause dilution of the atomic vapor and air entrainment. The latter may increase the background emission or cause chemical or quenching interferences. In an attempt to provide a more uniform and constricted volume of atoms for AFS measurements, the length of the outer quartz tubing was extended as shown in Figure 1. For both the AFS-1 and AFS-2 torches, the extension tube was constricted down to 10 mm i.d. When the diameter of this section was decreased to less than 10 mm, the acoustical noise level of the plasma increased, the narrow section of the extension tube attained melting temperature, and the tail flame dispersed at shorter distances above the torch tip. Tubes with extension diameters larger than 10 mm i.d. were required for forward RF power levels greater than about 1 kW. Atomic fluorescence observations were made just above the tube extension.

Sample Introduction and Gas Handling Systems. The sample introduction system consists of a right-angle pneu-

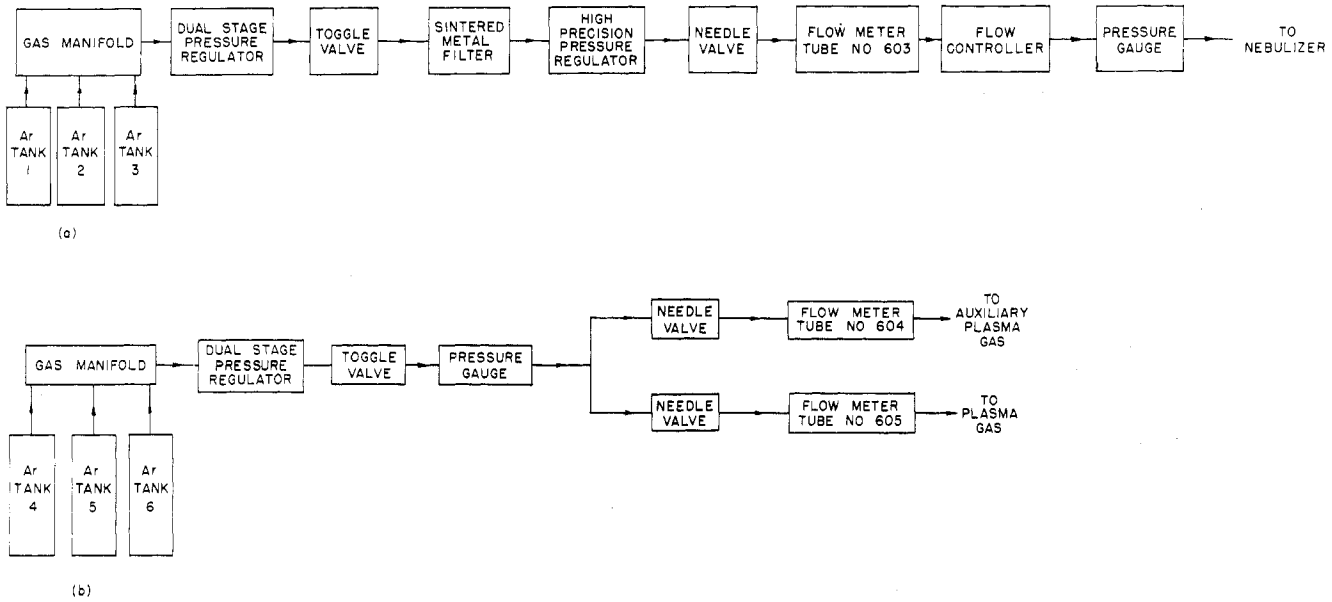

Figure 2. Block diagram of the gas handling system

(a) Aerosol carrier gas, (b) plasma and auxiliary gas

matic type nebulizer (*14*) and a dual tube aerosol chamber (*15*). The aerosol was fed directly to the plasma and no external desolvation apparatus was used. The efficiency of the sample introduction system (ml of solution delivered to the plasma/ml of solution nebulized) was about 3% for a nebulizer argon flow of 1.4 l./min (*15*). For all the experiments reported here, the nebulizer carrier gas (argon) flow rate was changed from 1 to 2.6 l./min by increasing the pressure drop across the nebulizer. As will be demonstrated in a later section, at higher argon flow rates, more aerosol entered the plasma and the AF signal increased.

Diagrams of the gas handling system employed for this ICP are shown in Figure 2. Because both AE and AF signals were more sensitive to aerosol carrier-gas flow than to plasma-gas flow variations, two independent sets of argon tanks were utilized for the two flow systems to maintain long term stability. The schematic diagram of the nebulizer-gas flow system is shown in Figure 2a. Three argon tanks were interconnected with a manifold equipped with station and check valves (Matheson Gas Products, Joliet, Ill.). A dual stage regulator (Model 93-250, Harris Calorific Co., Cleveland, Ohio) was used to reduce the tank pressure in two steps and to maintain constant upstream pressure. (Because large changes in the manifold pressure can cause noticeable changes in the aerosol-gas flow rate, even when dual stage regulators are employed, we have recently converted our gas-handling system to liquid Ar tanks. The low pressure in these tanks remains constant until essentially all of the Ar is used.) The sintered stainless steel filter (Model 1391, Brooks Instrument Division, Hatfield, Pa.) removed particulate matter that might impair the operation of the high precision pressure regulator, the needle valves, the flow controller, and the nebulizer. For proper functioning of the NRS flow controller (Model 8944, Brooks Instrument Division, Hatfield, Pa.), a high-precision pressure regulator (Model 8601B Brooks Instrument Division, Hatfield, Pa.), was inserted upstream of the flow meter (tube 603, Matheson Gas Products, Joliet, Ill.), and the flow controller. The latter served to maintain constant Ar flow to the nebulizer despite fluctuation in downstream pressure. A pressure gauge (0–60 psi) was added immediately upstream from the nebulizer to monitor the pressure drop across the nebulizer orifice.

The plasma–gas flow system, shown in Figure 2b, consisted of two channels. The system was similar to Figure 2a except that the filter, the high precision pressure regulator, and the flow controller were omitted. The auxillary gas flow (~1 l./min), which prevented overheating of the aerosol injection tube when the plasma was formed, was utilized *only* to initiate the plasma. The argon plasma-gas flow, which was normally 10 to 12 l./min, sustained the plasma and, in addition, provided thermal isolation and stabilization of the plasma. The entire gas handling system was calibrated with a wet test meter.

Radio Frequency Generator and Impedance Matching Network. Figure 3 shows a simplified diagram of the RF generator, the impedance matching network, the load coil, the plasma torch, the forward power regulator, and a pulsing network (not used in the present study). The RF generator consisted of a crystal-controlled oscillator and air-cooled power amplifier. The oscillation frequency was 27.125 MHz. The power output was adjustable to a maximum of 3 KW. The generator output was tuned for 50-Ω output impedance. Forward and reflected power could be monitored on two independent meters. A multimeter monitored the grid current, the plate voltage, and the filament voltage of the power tube. The RF power was delivered from the generator via a 50-Ω coaxial cable (RG115 Cable, Consolidated Wire and Associated Corporations, Chicago, Ill.) to the impedance matching network, which housed the variable capacitors for matching the plasma load to the transmission line. The coaxial cable was connected to the generator and the impedance matching network by means of RF connectors (Type HN, Amphenol RF Division, Danbury, Conn.). The impedance matching network was modified to reduce the high reflected power level; the values of the two variable capacitors C_1 and C_2 in the modified unit were 10 to 100 pF and 650 to 1100 pF, respectively.

The two-turn, water-cooled load coil was fabricated of 5-mm o.d. copper tubing. The coil diameter was ~30 mm and the center line to center line spacing was ~7 mm. The coil was attached directly to the front of the impedance matching network and protruded from its housing. The top turn of the coil was connected to the high voltage side of the system, as shown in Figure 3. The position of the load coil with respect to the torch center could be changed as described in a previous section. The length of the coil, measured from the coil center to the front of the impedance matching network, was ~130 mm.

Forward Power Regulator and the Pulsing Network. The

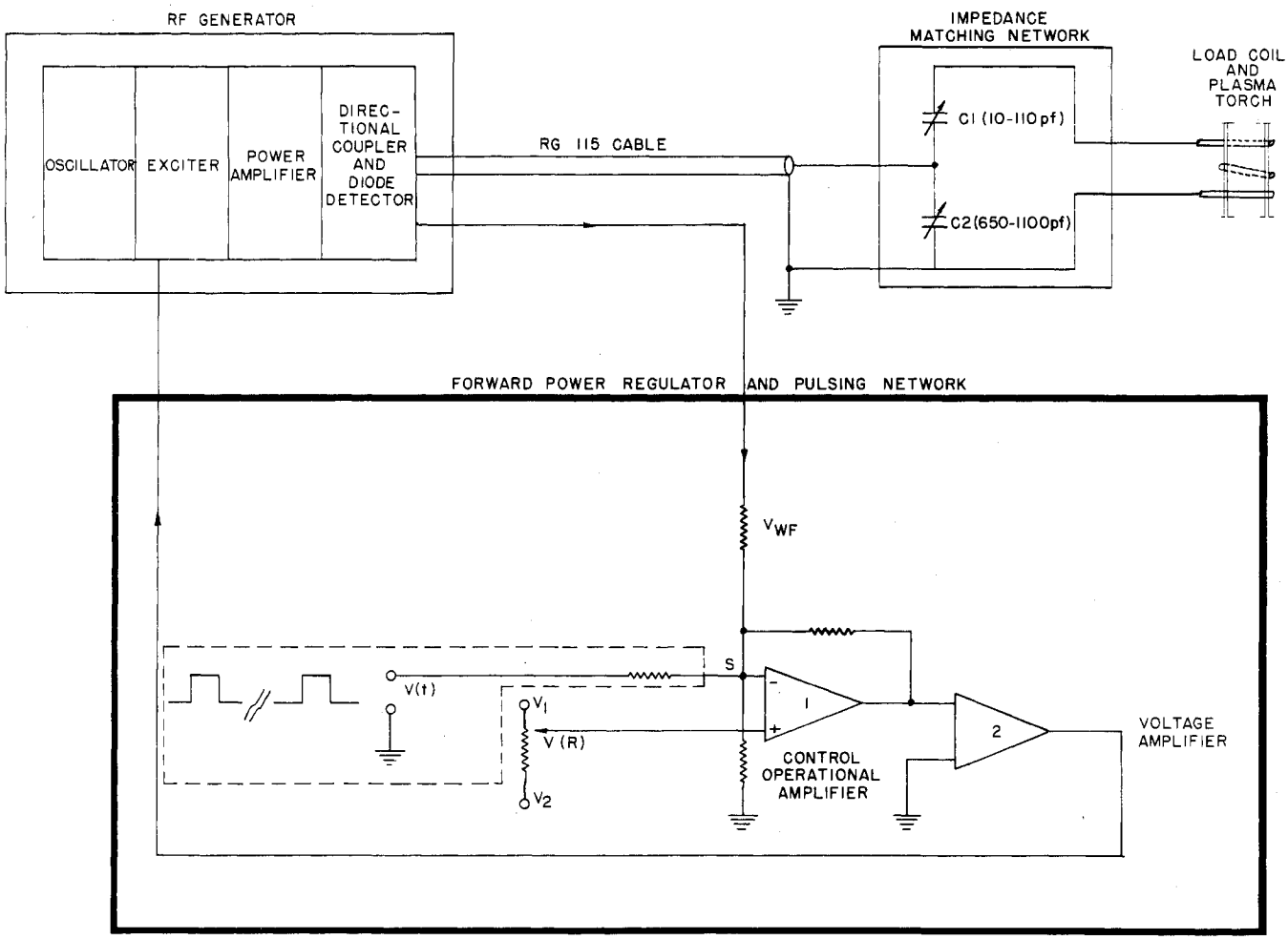

Figure 3. Simplified circuit diagram of the RF generator, the impedance matching network, the load coil, the forward power regulator, and the pulsing network

simplified circuit diagram of the forward power regulator and the pulsing network is shown in Figure 3. The directional coupler sampled the forward and reflected power on the transmission line. The diode detector converted the RF envelope to dc voltage representations of the forward (V_{WF}) and reflected (V_{WR}) power. For operation in the continuous mode, the operator selected the desired RF power level by adjusting the reference voltage $V(R)$. The control operational amplifier (OA) compared the forward component of the RF power V_{WF} and the reference voltage $V(R)$. The OA output was boosted to ~375 V by a voltage amplifier and was applied across the screen grids of the exciter tubes.

With an ideal system having low noise, high gain, and a linear transfer function, V_{WF} will track $V(R)$ approximately to $1/A_1 \cdot A_2 \cdot A_3 \cdot A_4$, where A_{1-4} are gains of the OA (volt/volt), voltage amplifier (volt/volt), RF unit (watt/volt) and directional coupler and detector (volt/watt). For computer control applications, a signal $V(t)$ may be fed to the summing junction S of the OA to program the power level as a function of time. This function is suitable for multielement analysis as well as operation in the pulse mode when AE and AF measurements are performed at high and low RF power levels, respectively.

Radiofrequency Grounding System. The RF generator and the impedance matching network were connected to a RF ground pipe via 1-cm o.d. soft copper tubings. In the final configuration, sharp bends in the copper tubing were avoided; the bend radii were at least 15 to 25 cm. The last 15 cm of each copper tube was flattened and horizontally wrapped around at least ¾ of the RF ground pipe circumference. All connections between the copper tubings and RF ground pipe were made by bolts and shake-proof washers. This configuration provided a low ground impedance for the RF.

The RF ground consisted of a 365-cm long, 5-cm o.d. galvanized steel pipe inserted in a hole drilled in the laboratory floor. The inside and the circumference of this tubing were filled with sand. Approximately 1 l. of water was introduced every 3 to 4 months in and around the pipe to ensure a very low ground impedance. Standard RF line filters were used on all electrical devices to reduce the RF interference level. The filters were particularly effective for the lock-in amplifier system.

Detection System and Associated Electronics. The photomultiplier output was converted to a proportional voltage by a remote preamplifier and fed to a lock-in amplifier tuned to the frequency of a mechanical chopper. The lock-in output was connected to the analog input channel of the ADC, and the analog signal was digitized and stored in the computer memory. The process was then repeated for a preset number of cycles (600 cycles in 18 ms), which represented one experiment. Under program control, the entire process could be repeated for a preset number of experiments after which the average value and standard deviation were calculated. Successive experiments were separated by 30-s time intervals.

The dc components of the signal resulting from analyte thermal emission, plasma background, and dark current were blocked by the lock-in amplifier. A separate blank determination was run on a deionized water blank prior to each ex-

Table II. Experimental Conditions for Atomic Fluorescence Studies

Spectrometer	1 meter Spectrometer, see Table I
Slit width	400 μm
Slit height	10 mm
Band pass	0.33 nm
Analytical wavelengths	228.8 nm(Cd), 213.8(Zn), 253.6(Hg)
Primary Excitation Source	Thermostated EDL, Cd(PNK), Zn(PNK), and Hg(OPH); see Table III for description.
PES Image width	0.3 cm
PES Image height	1 cm
PES Image width for detection limit determination	3 cm
Lock-In Amplifier	See Table I
Chopper frequency	260 Hz
Chopper duty cycle	50%
Time constant for optimization studies	3 s
Time constant for detection limit determination	30 s
Selectivity (Q)	5
Integration Time (see text)	18 ms
Photomultiplier Tube Voltage	1000 V
Analyte Concentration for Optimization Studies	10 μg/ml

Table III. Optimum Parameters[a] for Single- and Multiple-Element Thermostated EDL's Operated with an "A"-antenna

Element[b]	Elements in the lamp	Supplier[c]	Lamp length X width, mm X mm[d]	Optimum operating temperature, °C	Optimum microwave power, W	Temperature difference, °C[e]
Cd	Cd	PNK1	35 × 8	100	75	150
Cd	Cd	PNK2	40 × 8	170	100	80
Cd	Cd	SRC	46 × 10	230	112	20
Cd	Cd	JDW	40 × 10	250	112	0
Cd	Cd	OPH	25 × 10	250	50	0
Cd	Cd-Zn-Hg	OPH	25 × 10	400	38	150
Cd	Cd-Zn-Hg-Tl	OPH	25 × 10	300	38	50
Zn	Zn	PNK	40 × 8	320	62	10
Zn	Zn	JDW	40 × 10	420	50	110
Zn	Zn	OPH	25 × 10	400	50	90
Zn	Cd-Zn-Hg	OPH	25 × 10	400	38	90
Zn	Cd-Zn-Hg-Tl	OPH	25 × 10	300	38	10
Hg	Hg	PNK	85 × 8	30	87	20
Hg	Hg	SRC	43 × 10	30	125	20
Hg	Hg	OPH	33 × 10	30	112	20
Hg	Cd-Zn-Hg	OPH	25 × 10	200	38	150
Hg	Cd-Zn-Hg-Tl	OPH	25 × 10	100	38	50

[a] Optimum parameters for maximum atomic fluorescence radiance are listed in Table IV. [b] Analysis wavelengths for Cd, Zn, and Hg were 228.8, 213.8, and 253.6 nm, respectively. [c] PNK = P. N. Keliher, Villanova University, Villanova, Pa.; SRC = S. R. Crouch, Michigan State University, East Lansing, Mich.; JDW = J. D. Winefordner, University of Florida, Gainesville, Fla.; OPH = Ophthos Instrument Co., Rockville, Md. [d] These numbers refer to the lamp outer dimensions. [e] The literature optimum temperatures for Cd, Zn, and Hg are 250, 310, and 50 °C, respectively, for single- and multiple-element lamps (*17,18*).

periment and the results were stored in the computer. The computer then entered an integration routine (600 values of the digitized analog signal), and the integrated AF (or AE) signal, after blank subtraction, was printed on the teletype.

Preparation of Solutions. Stock solutions for Cd, Zn, and Hg were prepared from pure metals dissolved in minimum amounts of HCl or HNO_3. All solutions were stored in polyethylene and prepared within hours of use to minimize analyte absorption on the wall of the container. To prevent Hg loss from solutions, ~1% (V/V) HNO_3 and 0.002% (W/V) $KMnO_4$ were added as preservatives. The oxidizing environment of the acid–$KMnO_4$ mixture also reduced the long nebulizer-spray chamber clean-up time, which was only experienced for Hg solutions.

RESULTS AND DISCUSSION

Prior to obtaining analytical data for the AFS-ICP system, a variety of parameters, such as EDL temperature and EDL microwave power, the height of observation in the plasma, the aerosol carrier gas flow rate, the plasma gas flow rate, and the forward RF power into the plasma were optimized for maximum AF signal and high signal-to-noise ratio. For all results presented here, each EDL was operated at its optimum parameters, determined as described below. The remainder of the experimental conditions are given in Table II. Each data point consisted of the average of three to five successive determinations. A conventional torch was utilized for all results reported here. Similar data were obtained for other configurations; the results will be given at the conclusion of the optimization sections. All optimization results were verified by the Simplex method (*16*).

Primary Excitation Source Parameters. Table III shows a summary of the optimum operating parameters for the single-element lamps along with those for two different multiple-element lamps containing Cd-Zn-Hg and Cd-Zn-Hg-Tl. The last column in Table III provides the temperature

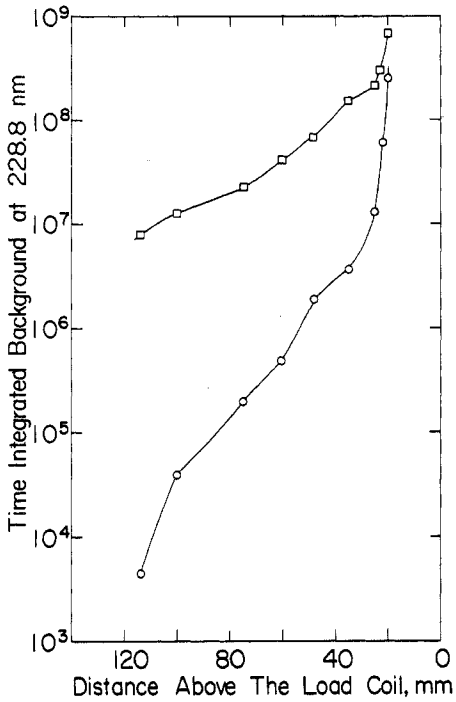

Figure 4. Plasma emission background in arbitrary units at Cd analysis wavelength as a function of observation height and forward RF power

(O) Forward RF power = 700 W; (□) forward RF power = 1000 W. In both cases, the plasma and aerosol-carrier gas flow rates are 9.4 and 2.4 l./min, respectively

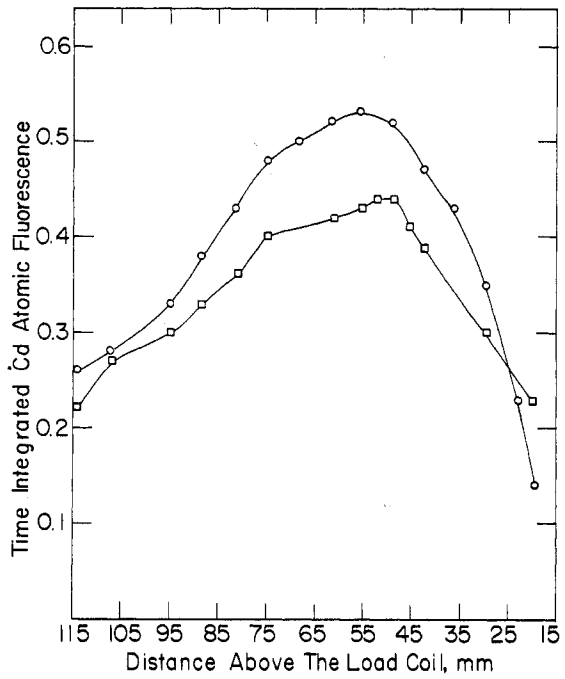

Figure 5. Cd atomic fluorescence in arbitrary units as a function of observation height and forward RF power

(O) Forward RF power = 800 W; (□) forward RF power = 1000 W. In both cases, the plasma and aerosol-carrier gas flow rates are 12.2 and 2.4 l./min, respectively

difference between these results and the literature. According to Browner and Winefordner (*18*), temperature differences of less than 30 °C may be considered as insignificant because variations in fill gas composition and pressure from lamp to lamp may account for differences of this magnitude. As shown by the data in Table III, we find disagreements of up to 150 °C with the literature optimum temperatures for single element lamps. Also, the observed optimum operating temperatures for each element in the two multielement EDL's differed by as much as 120 and 300 °C, respectively, for Zn and Cd, from those determined for one or more of the single element lamps. These findings are in disagreement with those reported by Patel et al. (*17*), who found that the optimum temperature for single element EDL's was approximately the same as that for multiple element versions. The lamp-to-lamp variation of optimum temperature for each element may be due to variation in the parameters such as the fill-gas composition and pressure, the lamp dimensions, the amount and the chemical form of the element in the lamps, and the care taken in the lamp preparation. As noted above, the fill-gas composition and pressure have been shown to cause temperature variations of about 30 °C (*18*). The effect of lamp dimension and the amount of an element (or compound) charged into the lamp has not been investigated for the thermostated EDL's thus far, but comparison of EDL length and width (see Table III) with optimum temperatures indicate that EDL dimensions should not cause the temperature variation for these particular lamps. Because the procedure for the addition of element (or compound) to the quartz tube is not quantitative (*19, 20*), different EDL's of the same element may contain different amounts of a particular element. Therefore, lamp to lamp temperature variation may be related to the amount and the chemical form of the element in the lamp.

Atomizer Parameters. *Influence of Observation Height and Forward RF Power on Plasma Background.* In AF spectrometry, the major noise source at the limit of detection is either the atomizer background flicker or dark noise (depending on the atomization cell used and the wavelength of interest). When an ICP is employed as an atomization device, radiofrequency interference (RFI) may influence the electronic system and may strongly interfere with the operation of the lock-in amplifier if the *entire* spectrometer is not properly grounded. In the absence of significant RFI, as was the case in the present study, the plasma background flicker is the major noise source. Since the root-mean-square shot noise current of a photomultiplier tube is directly proportional to the square root of phototube anode current, the influence of experimental parameters on the reduction of plasma background emission was investigated. Figure 4 illustrates the effect of forward RF power on the time integrated background at 228.8 nm as a function of observation height, which is taken as the distance above the load coil. For a forward RF power of 700 W, the background emission changed by about five orders of magnitude when the observation height was changed from 20 to 120 mm above the load coil. If the forward RF power was increased to 1000 W, the background emission was enhanced by about 3 orders of magnitude when the observation height was at about 120 mm from the load coil. However, the background emission was less sensitive to RF power variations when the observation window was moved close to the load coil. These observations showed that as far as background emission was concerned, AF measurements should be conducted at low power levels and at a distance well above the load coil.

Influence of Observation Height and Forward RF Power on Atomic Fluorescence. The Cd atomic fluorescence–height profiles for two forward RF power levels are shown in Figure 5. In contrast to the results obtained from background emission profiles, it can be seen that the optimum AF signal occurred at a distance 45 to 65 mm above the load coil. The maximum variation of the AF signal with height did not exceed a factor of five. A 20% increase in forward RF power causes an ~20% decrease in the AF signal. Forward RF power lower than 650 W caused plasma instability. It should be

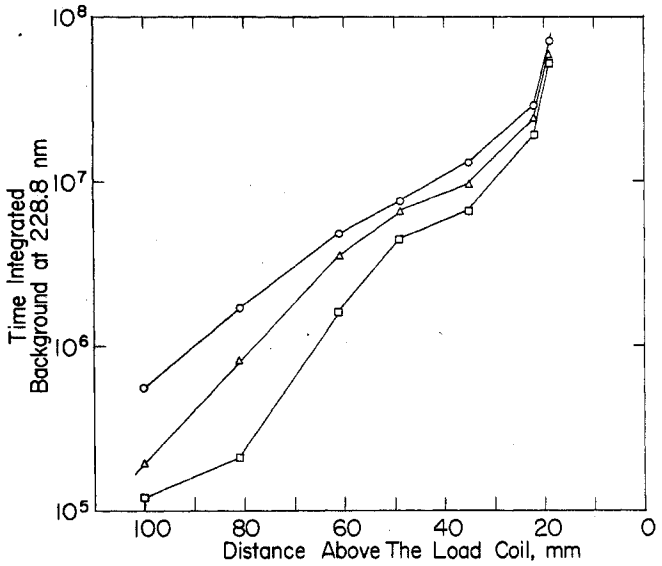

Figure 6. Plasma emission background in arbitrary units at Cd analysis line as a function of observation height and plasma–gas flow rate

(O) Plasma–gas flow rate = 12.1 l./min; (△) plasma–gas flow rate = 14.7 l./min; (□) plasma–gas flow rate = 21.7 l./min. The aerosol–carrier gas flow rate and the forward RF power in all cases are 2.4 l./min and 800 W, respectively

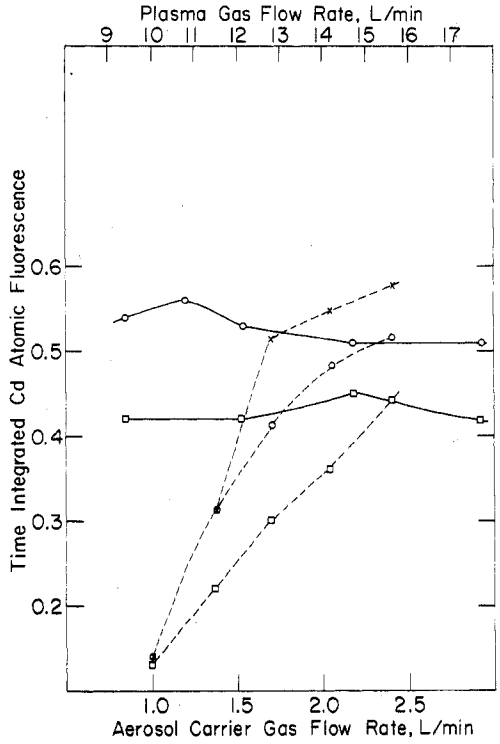

Figure 7. Cd atomic fluorescence signal as a function of plasma gas and aerosol–carrier gas flow rates, at various RF power levels

(X) Forward RF power = 700 W; (O) forward RF power = 800 W; (□) forward RF power = 1000W; (- - -) AF signal variation vs. aerosol–carrier gas flow rate (observation height = 55 mm above the load coil; plasma–gas flow rate = 10.8 l./min); (—) AF signal variation vs. plasma–gas flow rate (observation height = 55 mm above the load coil; aerosol–carrier gas flow rate = 2.4 l./min)

emphasized here that optical emission measurements are normally performed in these laboratories at 15 to 25 mm above the load coil and at forward RF power levels of 1000 to 1200 W when aqueous samples are analyzed.

For a given power level, the signal to root-mean-square noise ratio (SNR) in AF measurement reached a maximum at 45 to 65 mm above the load coil. At higher observation heights, the SNR was slightly lower. When the observation window was moved close to the load coil (15 to 30 mm above the load coil) the SNR was reduced significantly. Higher forward RF power generally reduced the SNR.

Influence of Plasma–Gas Flow and Aerosol–Carrier Gas Flow Rates on Plasma Background. The effect of plasma–gas flow rates on the background emission for a forward RF power of 800 W and aerosol–carrier gas flow of 2.4 l./min is illustrated in Figure 6. It can be seen that higher gas flow rate reduces the ICP background. As the observation window was moved closer to the load coil, the plasma background became a less sensitive function of plasma–gas flow rate. Similar results were obtained for aerosol–carrier gas flow variations.

Influence of Plasma–Gas Flow and Aerosol–Carrier Gas Flow Rates on Atomic Fluorescence Signal. The effect of plasma–gas flow rate on Cd atomic fluorescence is demonstrated by the unbroken line in Figure 7. These measurements were performed at the observation height of 55 mm above the load coil and for an aerosol–carrier gas flow rate of 2.4 l./min. The plasma–gas flow variation between 9 to 19 l./min caused only a small overall decrease in the AF signal, presumably arising from dilution of the atomic vapor. Furthermore, the SNR decreased with increase in the plasma–gas flow rate because of increased turbulence. As expected, higher RF power levels decreased the AF signal. For AF measurements, the optimum plasma–gas flow rate was about 10 to 12 l./min.

The variation of the AF signal as a function of the aerosol–carrier gas flow rate, for three forward RF power levels, is shown in Figure 7 by the dashed lines. The AF signal changed by a factor of 5 when the Ar flow rate was changed from 1 to ~2.4 l./min. At higher aerosol–carrier gas flow rates, more sample was introduced into the torch and the plasma background was reduced, presumably by the cooling effect of the higher aerosol–carrier flow rate and the presence of more water in the axial channel of the plasma. As a result, both the signal and SNR were greatly enhanced at higher flow. For the analysis of aqueous samples performed in this laboratory by AE, the plasma and aerosol–carrier gas flow rates have ranged from 10 to 12, and 1 to 1.4 l./min, respectively.

From the above observations, the following conclusions were drawn. First, the optimum height for performing AF measurements was located at a distance of 45 to 65 mm above the load coil. Second, higher RF power levels reduced the atomic fluorescence and the signal-to-noise ratio. Third, the plasma–gas flow rate had only a small effect on the analyte signal, but higher gas flow rates decreased the SNR and deteriorated the detection limit. Fourth, increases in the aerosol–carrier gas flow rate produced a significant increase in the net signal and the SNR.

These conclusions, based on AF observations with a conventional torch, led to the design of other torch configurations. Because higher aerosol–carrier gas flow rates and lower RF power may lead to incomplete atomization, a logical modification is to extend the outer tube so that the plasma–particle interaction time is lengthened (AFS-1 and AFS-2 torches).

The conclusions regarding the optimum parameters for the conventional torches were found to be generally valid for extended torches. However, experimental constraints (see Table IV) prevented a definitive determination of the true (or global) observation height optima for the extended torches. The plasma–gas flow rate was found to have a more pronounced effect on the AF radiance. For example, for a plasma–gas flow rate variation of 10 to 20 l./min, the AF signal was reduced by about 10%, 30%, and 40% for the conventional torch, AFS-1, and AFS-2 torches, respectively. In the conventional torch, mixing of the plasma gas and aerosol streams occurred only

Table IV. Parameters for the Determination of Cd, Zn, and Hg in Aqueous Solution with the AFS-ICP Spectrometer

Torch-Method	Observation height, mm	RF power, W	Plasma gas flow, l./min	Aerosol carrier gas flow, l./min[a]
Conventional Torch-AFS	45–65	700	10	2.4
AFS-1 Torch-AFS	55[b]–75	700	10	2.4
AFS-2 Torch-AFS	95[b]	700	10	2.4
Conventional Torch-AES	15	1100–1500	10–18	1

[a] Flow rate larger than 2.4 l./min was not possible with the present nebulizer. [b] The outer tube prevented measurement at lower observation height above the load coil.

Table V. Detection Limits (μg/ml) and Dynamic Range with AFS-ICP System. Excitation Source Image Area = 3 cm²

		AFS-ICP			AES-ICP			
Element	Analysis wavelength, nm	Detection limits	Linear concentration range above detection limit concentration	AFS-Flame (Air/H_2) The best detection limit reported (*19,20*)	Detection limit, present work	Ames Laboratory, best detection limits (*1*)	The best detection limits reported by other laboratories (*3*)	Improvement factor
Cd	228.8	0.0004	5×10^5	0.000001	0.002	0.002	0.0002	5
Zn	213.8	0.001	1×10^5	0.00004	0.002	0.002	0.0001	2
Hg	253.6	0.01	5×10^3	0.01	0.08	0.2	0.001	8

to a small extent; hence, the atomic vapor residence time should not have been influenced significantly. The narrow section of the extension tube in the AFS-1 and AFS-2 torches caused a significant mixing of the plasma and analyte streams with a consequent reduction in the atom residence time within the viewing field of the spectrometer.

Similar optimum parameters were also obtained for Zn and Hg. Table IV summarizes the optimum parameters for the various torches. A range of values is given for the height parameters for AFS; within experimental error, the measured detection limits were the same within these ranges. The optimum parameters employed for the detection of Cd, Zn, and Hg in aqueous solution by AE are also given. For the determination of optimum parameters in AE, the monochromator slit height and width were taken as 5 mm and 20 μm, respectively, and the entrance optics lens aperture was reduced to 5 mm.

Analytical Results. *Detection Limits and Dynamic Range.* The detection limits, defined as the concentration required to give a signal-to-root mean square noise ratio of 2, were determined for the conventional AFS torch, under the experimental conditions listed in Tables II, III, and IV. The values obtained for Cd, Zn, and Hg as well as the concentration ranges giving linear analytical calibration curves for these elements are given in Table V. Each detection limit determination represents 10 successive measurements of the signal and background levels. For AFS determinations, the primary excitation source image area on the plasma was increased to 3 cm² and a conventional torch was utilized. Similar detection limits were obtained for other torch designs. No improvement in detection limits (signal-to-noise ratios) was obtained when the 0.25-meter monochromator was utilized for AFS measurements. For comparison, the best reported AFS–flame detection limits (*9, 10*) and the AES-ICP detection limits obtained in this work at the corresponding optimum conditions (see Table IV) are presented along with the best results previously reported by this and other laboratories (*1, 3*). The final column in Table V provides the improvement factor of the AF detection limits over AE *when the same experimental facilities are used for both techniques.* The best improvement was obtained for Hg.

A comparison of the AFS results obtained with the air–H_2 flame and ICP indicates the superiority of this flame for the determination of Cd and Zn in matrix-free solutions. However, the low temperature of the air–H_2 flame may cause severe physical and chemical interferences in analysis of samples containing concomitants in addition to the analyte (*7*). If comparisons are drawn between the AFS-ICP result with AES-ICP data reported in column 8, it should be remembered that the two sample introduction and atomization systems were entirely different. AFS measurements with the Boumans–de Boer (*3*) system should provide improved detection limits.

Detection limits were also determined for Cd with a Perkin-Elmer EDL and for Cd and Zn with Osram lamp primary sources. It should be emphasized that the Perkin-Elmer EDL system was not thermostated. The Cd detection limit determined with this EDL at the recommended power level of 5 W was about 6 ng/ml, which was a factor of 15 inferior to the value determined with a thermostated system. This detection limit could be decreased to about 1.2 ng/ml if the lamp power level was increased to 8 W. At this power level, the lamp radiance was increased, but operation for about 15 min caused lamp and power supply overheating and an automatic shutoff. The Cd and Zn detection limits obtained with an Osram lamp operated at optimum lamp currents were about 10 and 8 ng/ml, respectively.

Primary Radiation Scattering and Matrix Interference Effects. The conventional and AFS-1 torches were used for all of the investigations presented in this section. The background signals arising from scatter of PES radiation at the Cd 228.8- and Zn 213.8-nm wavelengths by unvaporized water droplets and solute particles were measured as a function of observation height and under the conditions shown in Table IV. The scatter vs. height profiles were essentially flat when 10 000 μg/ml of Al as chloride was introduced into the plasma. Although no scattering signal was detected, the presence of the concomitants increased the baseline noise slightly.

The influence of 10 000-fold excesses of 17 species on the AF signals of 1 μg/ml Cd and Zn was measured at about 75 mm above the load coil, under the conditions shown in Table IV. The results expressed as percentage change with respect to the signals observed when the solutions contained only 1 μg/ml Cd or Zn are given in Table VI. Negative results indicate depression of the AF signal, which may be due to physical or chemical interference effects occurring in the nebulizer, in the

Table VI. Interferences in the AFS Determination of Cadmium (1 μg/ml) and Zinc (1 μg/ml) Using the AFS-ICP Spectrometer

Interferant	Salt	% Change in analyte AF signal from 10 000 μg/ml of Interferant: Cd, PESIA[a] = 0.3 cm²	PESIA[a] = 3 cm²: Cd	PESIA[a] = 3 cm²: Zn
Al	$Al_2(SO_4)_3$	+1	+1	−12
Ca	$CaCO_3/HNO_3$	−11	−8	−12
Co	$CoCl_2$	−17	−6	−15
Cr	$CrCl_3$	−6	−7	−7
Cu	$Cu(NO_3)_2$	−8	−7	−6
K	KCl	−3	−5	−4
Mg	$MgCl_2$	−9	−10	−7
Mn	$MnCl_2$	+1	−5	−5
Na	NaCl	−11	−12	−9
Ni	$NiCl_2$	−10	−10	−2
Pb	$Pb(NO_3)_2$	0	−3	−6
V	V/HNO_3	−4	−4	+1
Cl^-	HCl	0	−6	0
NO_3^-	HNO_3	0	0	0
PO_4^-	H_3PO_4	+1	0	0
SO_4^{2-}	H_2SO_4	−4	−4	0
CH_3COO^-	CH_3COOH	+1	+1	0

[a] PESIA = PES image area.

dual tube spray chamber, or in the plasma. Reference blank solutions containing the interferant but not the analyte did not provide a measurable AF signal. To determine if the interference effects were affected by the external optics, the interference studies for Cd were conducted for PES image areas of 0.3 and 3 cm² (see Table VI). A maximum depression of 17% occurred in the presence of $CoCl_2$, and the depression was about 10% for the presence of Al, Ca, Mg, Na, and Ni. For all other species, the interference effects were not significant (less than 5%). Positive results were small in *all* cases and were within the experimental error of the entire measurement. No significant change was observed when the PES image area was increased from 0.3 to 3 cm².

CONCLUSION

The inductively coupled plasma has been evaluated as an atomization cell for AFS. The optimization of the atomizer parameters with three torch designs indicates that high RF power and plasma–gas flow rates reduce the AF signal and the signal-to-noise ratio. In contrast, high aerosol–carrier gas flow rates may significantly improve the AF signal and the signal-to-noise ratio. The optimum observation height for a conventional torch is at 45 to 64 mm above the load coil.

No scattering effect was observed for up to 10 000 μg/ml of Al, but the baseline noise was slightly increased. Although the AF optimum parameters are significantly different from those used in optical emission, the AF signal was not significantly influenced when Cd and Zn were determined in the presence of 10 000 μg/ml of 17 species.

The AF detection limits for Cd, Zn, and Hg were found to be superior to those obtained by AE by a factor of 2 to 8. In principle, improvement in the AF detection limits should be realized if more analyte per unit time can be introduced into the plasma and if primary source radiances could be increased. The design and construction of intense EDL's for most elements can presently be considered as much art as science. Fundamental investigation of these sources may lead to the development of more intense EDL's in the future. There are two obvious refinements in the optical arrangements that may improve the AF powers of detection significantly. These refinements are: (a) a mirror behind the PES to collect more primary source radiation, and (b) a secondary source mirror behind the plasma discharge to increase the signal-to-noise ratio.

ACKNOWLEDGMENT

The authors express their appreciation to all those who helped them in this project. S. A. Goldstein collaborated in the designs of the optical table and part of the plasma assembly. The EDL's were provided by S. R. Crouch (Michigan State University, East Lansing, Mich.), P. N. Keliher (Villanova University, Villanova, Pa.) and J. D. Winefordner (University of Florida, Gainesville, Fla.). Thanks are given to R. N. Kniseley and the Ames Laboratory design engineers David Birlingmair, G. E. Holland, and H. D. Shank for their advice and assistance in various parts of this work, and to W. Haas for his suggestions during the preparation of this manuscript.

LITERATURE CITED

(1) V. A. Fassel and R. N. Kniseley, *Anal. Chem.*, **46**, 1110A, 1155A (1974).
(2) S. Greenfield, I. Ll. Jones, H. McGeachin, and P. B. Smith, *Anal. Chim. Acta*, **74**, 225 (1975).
(3) P. W. J. M. Boumans and F. J. De Boer, *Spectrochim. Acta, Part B*, **30**, 309 (1975).
(4) J. D. Winefordner and T. J. Vickers, *Anal. Chem.*, **36**, 161 (1964).
(5) J. D. Winefordner and R. A. Staab, *Anal. Chem.*, **36**, 165 (1964).
(6) J. D. Winefordner, *Chem. Technol.*, 123 (1975).
(7) R. F. Browner, *Analyst (London)*, **99**, 1183 (1974).
(8) M. B. Denton and H. V. Malmstadt, *Appl. Phys. Lett.*, **18**, 485, (1971).
(9) L. M. Fraser and J. D. Winefordner, *Anal. Chem.*, **43**, 1693 (1971).
(10) N. Omenetto, L. M. Fraser, and J. D. Winefordner, *Appl. Spectrosc. Rev.*, **7** (2), 147 (1973).
(11) J. Kuhl and H. Spitschan, *Opt. Commun.*, **7**, 256, (1973).
(12) J. Kuhl, G. Marowsky, P. Kuntsmann, and W. Schmidt, *Z. Naturforsch, A.*, **27**, 601 (1972).
(13) R. F. Browner, B. M. Patel, T. H. Glenn, M. E. Rietta, and J. D. Winefordner, *Spectrosc. Lett.*, **5**, 311 (1972).
(14) R. N. Kniseley, H. Amenson, C. C. Butler, and V. A. Fassel, *Appl. Spectrosc.*, **28**, 285 (1974).
(15) R. H. Scott, V. A. Fassel, R. N. Kniseley, and D. E. Nixon, *Anal. Chem.*, **46**, 75 (1974).
(16) S. L. Morgan and S. N. Deming, *Anal. Chem.*, **46**, 1170 (1974).
(17) B. M. Patel, R. F. Browner, and J. D. Winefordner, *Anal. Chem.*, **44**, 2272 (1972).
(18) R. F. Browner and J. D. Winefordner, *Spectrochim. Acta, Part B*, **28**, 263 (1973).
(19) K. E. Zacha, M. P. Bratzel, J. D. Winefordner, and J. M. Mansfield, *Anal. Chem.*, **40**, 1733 (1968).
(20) D. O. Knapp, C. J. Molnar, and J. D. Winefordner, *Anal. Chem.*, **46**, 622 (1974).

RECEIVED for review June 5, 1975. Accepted May 7, 1976. This research was funded by the U.S. Energy Research and Development Administration under contract No. W-7405-Eng-82.